Vietnam Journal of Earth Sciences, 42(2), 118–129, Doi: 10.15625/0866-7187/42/2/14951

(VAST)

Vietnam Academy of Science and Technology

Vietnam Journal of Earth Sciences

http://www.vjs.ac.vn/index.php/jse

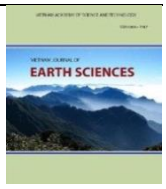

Fort-Dauphin beach sands, south Madagascar: Natural radionuclides and mineralogical studies

Hao Duong Van[1*], Alinanja Lantoarindriaka[2], Adam Piestrzyński[2], Phan Trong Trinh[3,4,5]

[1]*University of Mining and Geology, North Tu Liem, Hanoi, Vietnam*
[2]*AGH University of Science and Technology, Krakow, Poland*
[3]*Institute of Geological Sciences, VAST, Hanoi, Vietnam*
[4]*Royal Academy for Oversea Sciences, Brussels, Belgium*
[5]*Graduate University of Science and Technology, VAST, Hanoi, Vietnam*

Received 01 November 2019; Received in revised form 10 March 2020; Accepted 03 May 2020

ABSTRACT

The Fort-Dauphin beach sand placer occurs as black sands on the East-South of Madagascar. The placer contributes 2/3 of the total heavy mineral resources of this country. The major minerals of the deposit are monazite, zircon, quartz, garnet, spinel, sillimanite as non-refractory minerals; ilmenite, anatase, rutile, titanite, leucoxene, pseudorutile and as a refractory one. The average concentration of the ilmenite, monazite, zircon and other minerals is 66.72%, 2.3%, 2.8%, and 28.18% respectively. Ilmenite contains 63 wt.% of TiO_2, Zircon-44 wt.% of ZrO_2, Monazite contains 53 wt.% of oxide rare earth elements (REE) and up to 2 wt.% of UO_2 and 9 wt.% of ThO_2. The total REE in the studied samples was observed high concentration up to 16000ppm and a high ratio of Σ LREE/Σ HREE>31. The principal natural radionuclide in this placer is 232Th with the concentration of 232Th from 2710 to 6000 ppm, 3620 ppm on average while for the 238U from 124 to 340 ppm, 237 ppm on average which are higher than the average of their in Earth's crust 360 and 70 times respectively.

Keywords: Fort-Dauphin beach sands; Natural radionuclides; disequilibrium; monazite; heavy minerals.

1. Introduction

The natural isotopes of 238U, 232Th, and their progeny principally contribute to terrestrial natural background radiation. The concentrations of the isotopes depend on the rock lithology, mineral compositions and underground water movement (Qu Limei et al., 2008; Strezov et al., 2009; Chau et al. 2008a; 2009; 2016). In many regions of beach sand placers, the high natural radionuclide concentration is observed, namely in India, Egypt, Greece, Brazil and Bangladesh (Mohanty et al., 2003a; Abd El Wahab & El Nahas, 2013; Takayuki et al., 2015; Papadopoulos et al., 2016). Deposits often contain monazite, zircon, ilmenite, garnet and so on, they were formed by long time weathering and erosion of different rock types, transported and deposited along the beaches. Many beach sand placers were studied by several scientists especially the

*Corresponding author, Email: haodnth@gmail.com

natural radionuclides and heavy elements in different regions such as Chhatrapur and Erasama beach placer deposit of Orissa in India; beach sand of Rosetta in Egypt; Placer Sands in Southeast Bangladesh; beach sands in Ilha Grande of Brazilian southeastern; beaches of Kavala, Sithonia Chalkidiki, Maronia, Samothraki, Mykonos of Greece: (Mohanty et al., 2003b; Freitas and Alencar, 2004; Mohanty et al., 2004; Sengupta et al., 2005; Alencar & Freitas, 2005; Sulekha et al., 2009; Nada et al., 2012; Abd El Wahab & El Nahas, 2013; Takayuki, et al., 2015; Papadopoulos et al., 2014a, b; 2015a, b; 2016). Moreover, the deposits of this type can often contain a high amount of rare earth elements (REE) also (Alam et al., 1999; Freitas and Alencar, 2004). For each beach sand placer, the radioactive, chemical and mineral characteristics will be different which will contain unique and interesting knowledge. The characteristics were depended on different original, environment and natural conditions. The Fort-Dauphin beach sand placer on the East-South of Madagascar is one of the biggest placers which contributes 2/3 of the total heavy mineral resources of this country. In this paper, authors attempt to study mineral composition, REE and natural radionuclides in the sand samples from Fort-Dauphin beach sand placer on the East-South of Madagascar.

2. The studied placer

The Fort-Dauphin beach sand placer is located in Flandrian Dunes surrounded by the Vohimena Mountains and the Indian Ocean in South-East of Madagascar Island (Fig. 1).

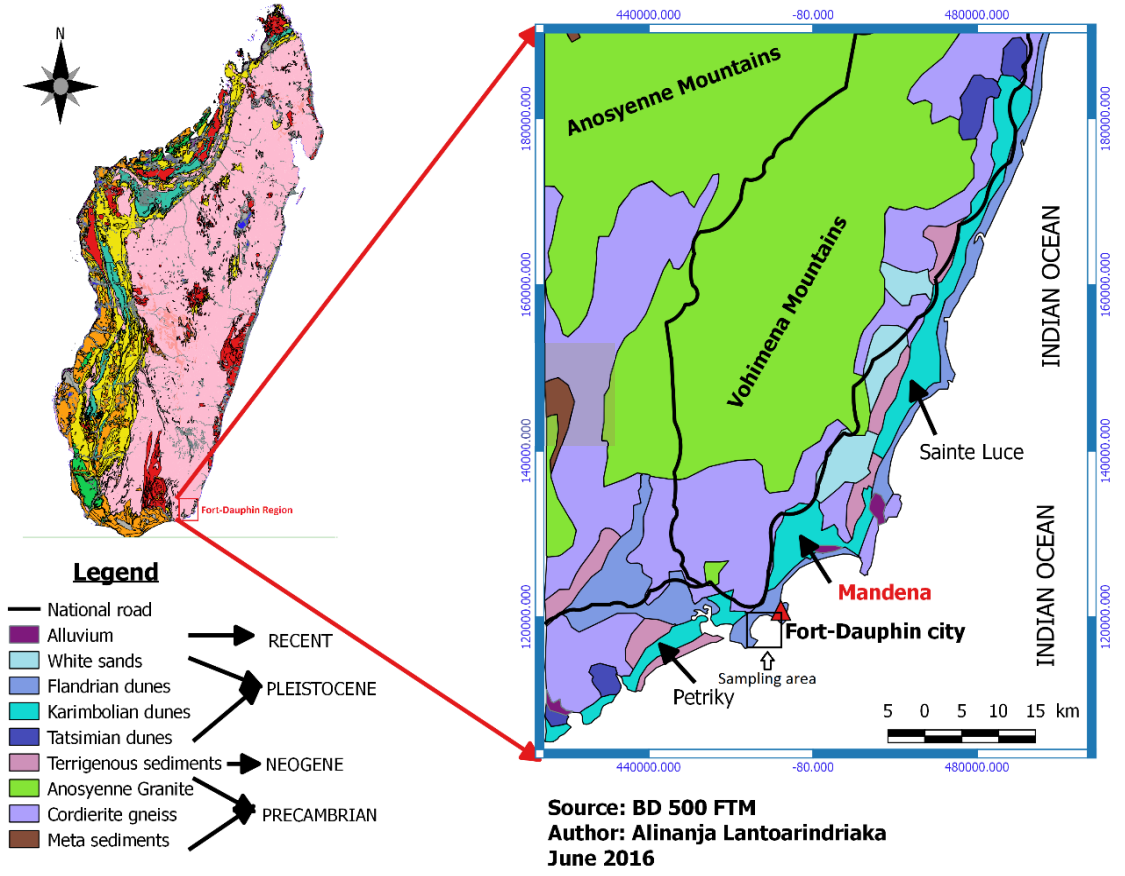

Figure 1. Geological map of the study area, modified from BD 500 FTM map (2016)

In the studied region, there are igneous, metamorphic and sedimentary formations. The igneous formation occupies the majority part of the Fort-Dauphin region and consists of the Vohimena and the Anosyenne Mountains granitic complexes. The essential compositions of the granitic complex are charnockite and garnet-biotite granite with a few dozen meters of lenses containing apatite-biotite, zircon and large crystals of monazite. The Anosyenne granite is composed of ilmenite, monazite, and magnetite (Andriamanantena, 2008). The coastal sedimentary formation consists of heavy minerals transported from eroded Anosyenne granite. Due to the potassium feldspar alteration, greenish-yellow color is observed along with the formation (Lacroix, 1922). The metamorphic formation in this area is characterized by the banded gneiss with biotite, cordierite, spinel, sillimanite, garnet, orthoclase and plagioclase (Bazot, 1974). The placer is very rich in titanium mineral accompanied by minerals bearing natural radioactive and heavy elements. The placer has been exploited by Rio Tinto Qit Madagascar Mineral QMM Company.

3. Materials and methods

3.1. Collection and pre-treatment of the samples

The six representative sand samples were collected from dune zones at the Fort-Dauphin beach sand placer. Each sample collected weighed approximately 600g and was collected from 0 to 20 cm in depth, mixed and homogenized. In the laboratory, the samples were divided into two parts, one for gamma measurement and the second for mineralogical and chemical study. The sample for gamma measurement was milled until the grains became less than 2 mm, then it was dried in an oven at 120°C for 24 hours to ensure that moisture was completely removed, then weighted accurately and packed in an aluminum cylindrical beaker of 120 ml capacity and sealed to prevent the escape of radon. The weighed and tightly sealed samples were left for at least 22 days to reach a secular equilibrium between ^{222}Rn and ^{226}Ra in the samples (Jodlowski & Kalita, 2010). After the stored period, the samples were measured using a gamma spectrometer with an HPGe detector. Samples for mineralogical and chemical studies were analyzed by the binocular and reflected light microscopes and ICP-MS. Heavy minerals were determined and separated as magnetic, semi-magnetic and non-magnetic fractions using a hand-magnet and a Frantz isodynamic separator.

3.2. Gamma spectroscopic analysis

The concentrations of ^{238}U and ^{232}Th were determined using gamma-ray spectrometer coupled with HPGe detector of the relative efficiency of 42% and resolution of 1.9 keV for 1332 keV line. The gamma spectrometer was calibrated using the IAEA reference materials RGU, RGTH, RGK as standard samples.

The gamma lines of 1000.8 keV (0.7%) from ^{234}Pa was used to determine the activity concentration of ^{238}U while that of ^{232}Th were determined from the gamma lines of 911.2 keV (29.0%) and 969.0 keV (2.3%) from ^{228}Ac and 583.0 keV (30.9%) and 2614.4 keV (35.8%) from ^{208}Tl (ICRP, 1983; IAEA, 1989). The ^{40}K concentration in the studied samples after subtract the amount contribute from ^{28}Ac is very low, it is not possible to determine ^{40}K concentration using gamma spectrometry in this case (with the very high uncertainties). Such high uncertainty is related to the interference of gamma rays of 1458.5 keV emitted from the ^{228}Ac so the ^{40}K concentration was neglected. The maximum counting time for every sample was 50 hours and the obtained uncertainty was less than 3% for low active samples. The self gamma absorption resulted from the difference in density of the studied samples and standard ones were introduced to follow the method

described by Jodlowski (2006). To avoid the photo effect absorption in the sample, all of the gamma lines were used higher than 500 keV.

The activity concentrations of ^{40}K, ^{226}Ra and ^{232}Th is calculated by formula (1) (Jodlowski, 2006).

$$A_{sp} = \frac{N_{sp} M_{st} A_{st} C_i}{N_{st} M_{sp}} \quad (1)$$

Where: N_{sp}, M_{sp} and N_{st}, M_{st} are the net measured intensity and mass of the sample and standard sample respectively, A_{st} is activity concentration of standard sample, C_i - the corrected factor for the differences between the densities of the sample and standard sample.

3.3. Energy-Dispersive X-Ray Spectroscopy

Analyses of ore minerals were carried out using an ore microscope and EDS systems consist of a sensitive X-ray semiconductor detector and liquid nitrogen for cooling. The EDS systems are combined with an electron scanning microscope FEI Quanta-200 FEG and software to analyze energy spectra at the Department of Mineralogy, Petrography and Geochemistry at the Faculty of Geology, Geophysics and Environmental Protection (FGGEP), AGH-UST (FGGEP AGH-UST). The principle of working of the instrument relies upon a high-energy beam (charged particles such as electrons, protons or X-rays) which is focused on small size by an electromagnetic lens with increased acceleration by high voltage (30 keV) shot into the sample being studied. The incident beam can excite an electron from the inner shell by interaction. An electron from an outer higher-energy shell fills the hole of an electron ejected. The result is emitted three principal signals include X-rays, backscattered electrons and secondary electrons. Those signals, the secondary electrons (SE) is used mainly for topography and in this study, the backscattered electron is used for mainly for chemical analysis such as pictures in the SEM display compositional contrast that results from different atomic number elements and their distribution and X-rays are used for chemical analysis. The number and energy of the specific X-rays emitted from samples can be measured by an EDS with a semiconductor detector. The energies of the X-rays are released with the characteristic of the difference in energy between the shells and of the atomic structure, EDS can determine the elemental composition of the samples. Base on X-rays of the K series consists of two recognizable lines Kα and Kβ for energies above 3 keV; the L series consists of Lα (1), Lβ1(0.7), Lβ2(0.2), Lβ3(0.08), Lβ4(0.05), Lγ1(0.08), Lγ3(0.03), Lλ(0.04), and Lη(0.01); the M series consists of Mα (1), Mβ (0.6), Mγ(0.05), Mζ(0.06), and MIINIV(0.01). The EDS is powerful and have useful form for qualitative analysis, specially, for heavy elemental analysis (elements heavier than beryllium). The technique with 130 eV; 0.1%; ±0.1% and 1–5 μm^3 is energy resolution (full width half max) at Mn Kα; limit of detection; precision and spatial resolution.

3.4. Inductively Coupled Plasma Mass Spectrometry

Chemical analyses of the studied samples were carried out by using the Aqua Regia digestion Ultratrace ICP-MS analysis method at ACME Labs-Bureau Veritas Commodities Canada Ltd. First, the sample is digested into a liquid state by acid. Then this liquid is pumped into a nebulizer, the nebulizer converts liquids into an aerosol, and that aerosol is transported into the plasma torch chamber where it is ionized. The ions from the plasma are extracted through a series of cones into a quadrupole (a mass spectrometer). Those ions are separated on the basis of their M/Z ratio (mass-to-charge ratio) and a detector receives an ion signal proportional to the concentration of the adequate element. The concentration of chemical elements in the analytical samples can be determined through calibration with multi-element reference standards.

4. Results and discussions

4.1. Natural radionuclides characteristic

The measured concentrations of ^{238}U and ^{232}Th are presented in (Table 1) which ranges from 124 ppm to 340 ppm, 237 ppm on average and 2710 ppm to 6000 ppm, 3620 ppm on average respectively. The ^{238}U and ^{232}Th concentration in studied samples are higher than the average of their in Earth's crust 70 and 360 times which are equal to 3.5 ppm and 10 ppm for 238U and ^{232}Th respectively (Lange 1972). There is a lack of data concerning with ^{40}K after eliminating the interference of the thorium progeny in Table 1, the fact is connected with the very low concentration of this isotope after correction of the interference of the gamma line originating from ^{228}Ac which contribute in gamma line of ^{40}K. So it is not possible to determine ^{40}K concentration using gamma spectrometry in this study and was not included with the estimated effective dose rate due to insufficient concentration of this isotope in the samples. The high concentration of ^{238}U and ^{232}Th in the study samples implies that the U and Th are the principal natural radioactive elements occurring in heavy minerals from the beach sand, while the activity concentration of ^{232}Th is higher than ^{238}U by five times, equivalent to fifteen times in mass. It is similar to some beach sand heavy mineral deposits in Australia (Elsner, 2010; Dean, 2011). This beach sand contributes heavy mineral and high concentration of radionuclides also, it is happening in different regions in worldwide and were being studied by many scientists such as (Mohanty et al., 2004; Sengupta et al, 2005; Alencar & Freitas, 2005; Sulekha et al, 2009; Nada et al., 2012; Abd El Wahab & El Nahas, 2013; Takayuki, et al., 2015; Papadopoulos et al., 2014a, b; 2015a, b; 2016).

Table 1. ^{238}U, ^{232}Th, REEs and chemical concentration in the studied samples (number of samples n=6)

Element	Unit	Min	Max	Average	Element	Unit	Min	Max	Average
Si	wt%	nd	nd	6.9	Sc	ppm	34.7	52	40.9
Al	wt%	0.38	0.98	0.54	Y	ppm	123	183	148
Fe	wt%	18.2	20.6	19.1	La	ppm	>2000	3140	nd
Mg	wt%	0.25	0.54	0.36	Ce	ppm	>2000	6900	nd
Ca	wt%	0.14	0.53	0.28	Pr	ppm	790	1600	1128
Na	wt%	0.07	0.12	0.09	Nd	Ppm	>2000	2830	nd
K	wt%	0.01	0.04	0.02	Sm	Ppm	384	782	555
Ti	wt%	8.5	25.5	14.2	Eu	Ppm	1.85	3.7	2.62
P	wt%	0.4	0.27	0.35	Gd	Ppm	203	326	247
Mn	ppm	2320	2550	2470	Tb	Ppm	14.6	33.4	22.7
Cr	ppm	206	280	231	Dy	Ppm	44	93.4	65
Ba	ppm	840	990	930	Ho	Ppm	3.3	4.8	3.9
Co	ppm	41.9	43.1	42.6	Er	Ppm	9	15.1	11.1
Ni	Ppm	1.4	15.5	10.5	Tm	Ppm	0.8	1.53	1.14
Ga	ppm	16.9	35.5	27.2	Yb	Ppm	5.9	11.8	8.8
Hf	ppm	14	745	258	Lu	Ppm	0.3	1.98	0.86
Nb	ppm	744	>1000	nd	W	ppm	8.5	11	9.7
Rb	ppm	0.51	1.5	0.97	Zn	Ppm	14	296	190
Sn	ppm	8.8	13	10.3	As	Ppm	0.7	13	8
Sr	ppm	73	95	82	Mo	Ppm	0.4	10.4	7
Ta	ppm	22.9	62.7	36.6	Pb	Ppm	61	287	195
Sb	Ppm	0.6	0.7	0.65	V	ppm	398	680	500
Au	Ppm	nd	0.7	nd	Zr	ppm	460	31000	10630
Cu	Ppm	5.7	36.6	25.8	Th-232	ppm	2710	6000	3620
Li	Ppm	6.3	7.7	7	U-238	ppm	124	340	237

4.2. Mineralogical characteristic

Three fractions were distinguished: non-magnetic, semi-magnetic and magnetic. Ilmenite occurs in the magnetic fraction which contributes 66.72% of the total samples. Ilmenite and its alteration products are the principal heavy minerals and participate in about 80% in this fraction. The monazite occurs in the semi-magnetic fraction, of which contribution amounts to 2.3% of the total sample and monazite participation occupies 67% in this fraction. Zircon mineral is the non-magnetic fraction which amounts to 2.8% of the total sample, and zircon occupies approximately 23% of non-magnetic fractions (Table 2). The quartz, zircon, garnet, spinel, sillimanite, monazite, anatase, rutile, titanite, leucoxene, pseudorutile and ilmenite are heavy minerals observed under the microscope. The reflected light pictures of the main minerals are shown in Fig. 2. Zircon occurs as very fine grains from 0.10 to 0.25 mm with a very well-shaped tetragonal system. Monazite looks as very fine rounded crystals pale of the dark yellow color. Magnetite occurs as an accessory mineral in the magnetic fraction. The chemical compositions of monazite, ilmenite, and zircon were analyzed by Energy-Dispersive X-Ray Spectroscopy (EDS) and are presented in Table 3 with typical monazite EDS spectrum in Fig. 4. The BSE images of the studied minerals are shown in Fig. 3. The average concentrations of the main oxide in monazite are $(REE)_2O_3$ – 52.2 wt.% while Ce_2O_3, La_2O_3, and Nd_2O = is 11.3 wt.%, 24 wt.% and 11.5 wt.% respectively, ThO_2 – 7.19 wt.% and UO_2 – 1.51 wt.%. In addition, the trace elements such as TiO_2 – 4.4 wt.% and Fe_2O_3 – 3 wt.% were recorded. The chemical analyses show that the monazite is very rich in natural radioactive elements in comparison to zircon and Ilmenite which contain less than detected limit by EDS method. Ilmenite contains 63 wt.% of TiO_2, and 22.4 wt.% of Fe_2O_3 with small impurities of Al_2O_3, CaO, MnO; Zircon contains 43.5% wt.% of ZrO_2 and few wt. % of HfO_2, TiO_2, and Fe_2O_3 but no radioactive elements were observed (see EDS spectrum Fig. 5a, b).

Table 2. The principal mineral contents

Valuable minerals	Wt. % (in beach sand)	Magnetic properties
Ilmenite	66.72	Magnetic
Monazite	2.30	Semi-magnetic
Zircon	2.80	Non-magnetic
Other minerals	28.18	Semi-magnetic Non-magnetic

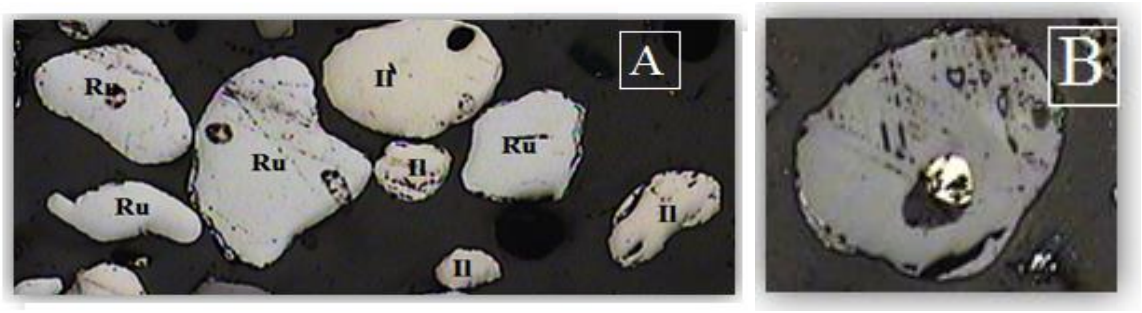

Figure 2. A, B, C: Mineral identification in feeds: A: ilmenite (Il) and rutile (Ru) (magnification 150 times). B: rounded grain of zircon (magnification 600 times). C: from left to right, ilmenite grain replaced by hematite and rutile mixture, (left edge), dark is silicate mineral (magnification 300 times). D, E, F, G: Mineral identification of magnetic fraction concentrates: D: intergrowth of ilmenite (light brown) with hematite (light grey) = hemo-ilmenite (magnification 600 times). E: Ilmenite with pseudorutile (pseudorutile occurs at the ilmenite boundary) (magnification 300 times). F: ilmenite with leucoxene (leucoxene sugary texture) (magnification 600 times). G: Ilmenite with silicate inclusion (magnification 600 times)

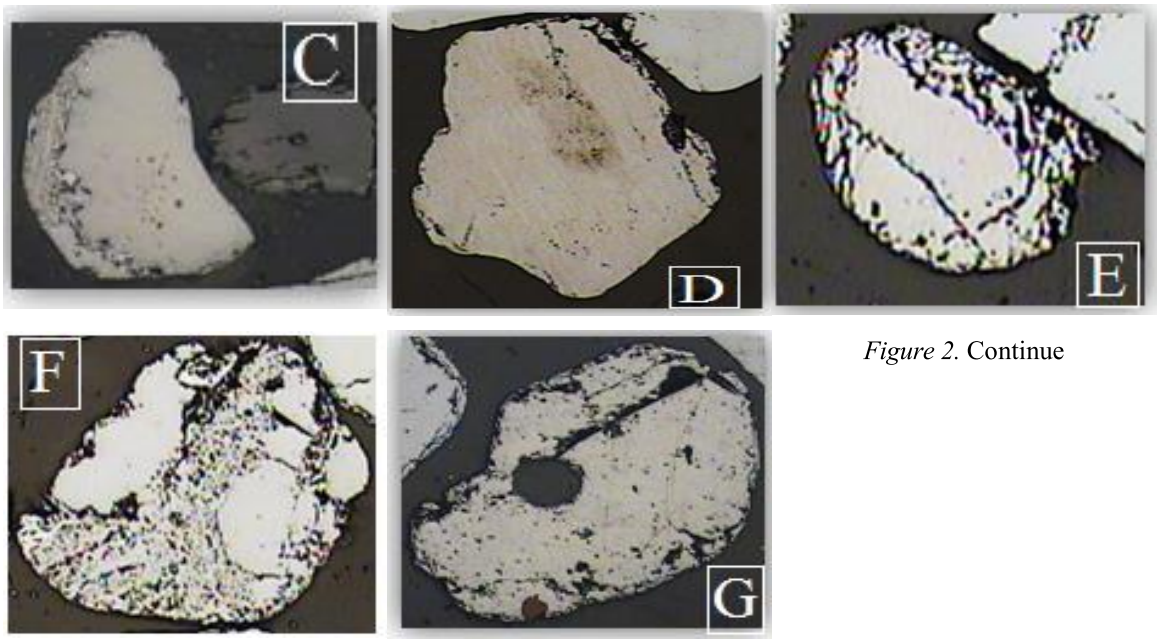

Figure 2. Continue

Table 3. EDS results-oxides Monazite-Ilmenite-Zircon corresponding BSE image points (number of table columns)

1		2		3		4		5	
Oxides	Wt. %	Oxides	Wt. %	Oxides	Wt.%	Oxides	Wt.%	Elements	Wt. %
P_2O_5	26.71	P_2O_5	27.28	P_2O_5	27.83	Fe_2O_3	22.44	Fe_2O_3	3.92
CaO	1.05	CaO	0.98	CaO	1.05	TiO_2	63.04	TiO_2	6.4
TiO_2	4.12	TiO_2	5.04	TiO_2	4.14	Al_2O_3	8.47	SiO_2	44.85
Fe_2O_3	3.08	Fe_2O_3	2.88	Fe_2O_3	3.04	P_2O_5	4.34	Hf_2O_3	1.31
Rb_2O	0.99	Rb_2O	0.81	Rb_2O	0	CaO	1.09	ZrO_2	43.52
AgO	0.21	AgO	0	AgO	0	MnO	0.62		
ThO_2	6.13	ThO_2	6.7	ThO_2	8.75				
UO_2	0.93	UO_2	1.98	UO_2	1.65				
PbO_2	1.34	PbO_2	1.15	PbO_2	1.49				
La_2O_3	10.76	La_2O_3	12.73	La_2O_3	10.4				
Ce_2O_3	23.43	Ce_2O_3	24.17	Ce_2O_3	24.59				
Pr_2O_3	3.36	Pr_2O_3	2.95	Pr_2O_3	3.57				
Nd_2O_3	13.24	Nd_2O_3	9.02	Nd_2O_3	12.22				
Sm_2O_3	1.65	Sm_2O_3	0.8	Tm_2O_3	0				
Gd_2O_3	0.6	Gd_2O_3	0.62	Gd_2O_3	0,84				
Dy_2O_3	0.16	Dy_2O_3	0.82	Dy_2O_3	0				
Lu_2O_3	0	Lu_2O_3	0.63	Ga_2O_3	0.19				
TaO	0.32	TaO	0.52	TaO	0.28				
GeO_2	0.45	GeO_2	0.52						
Total	98.53	Total	99.61	Total	99.20	Total	100	Total	100

Order number of columns are corresponding BSE image points in Fig. 3

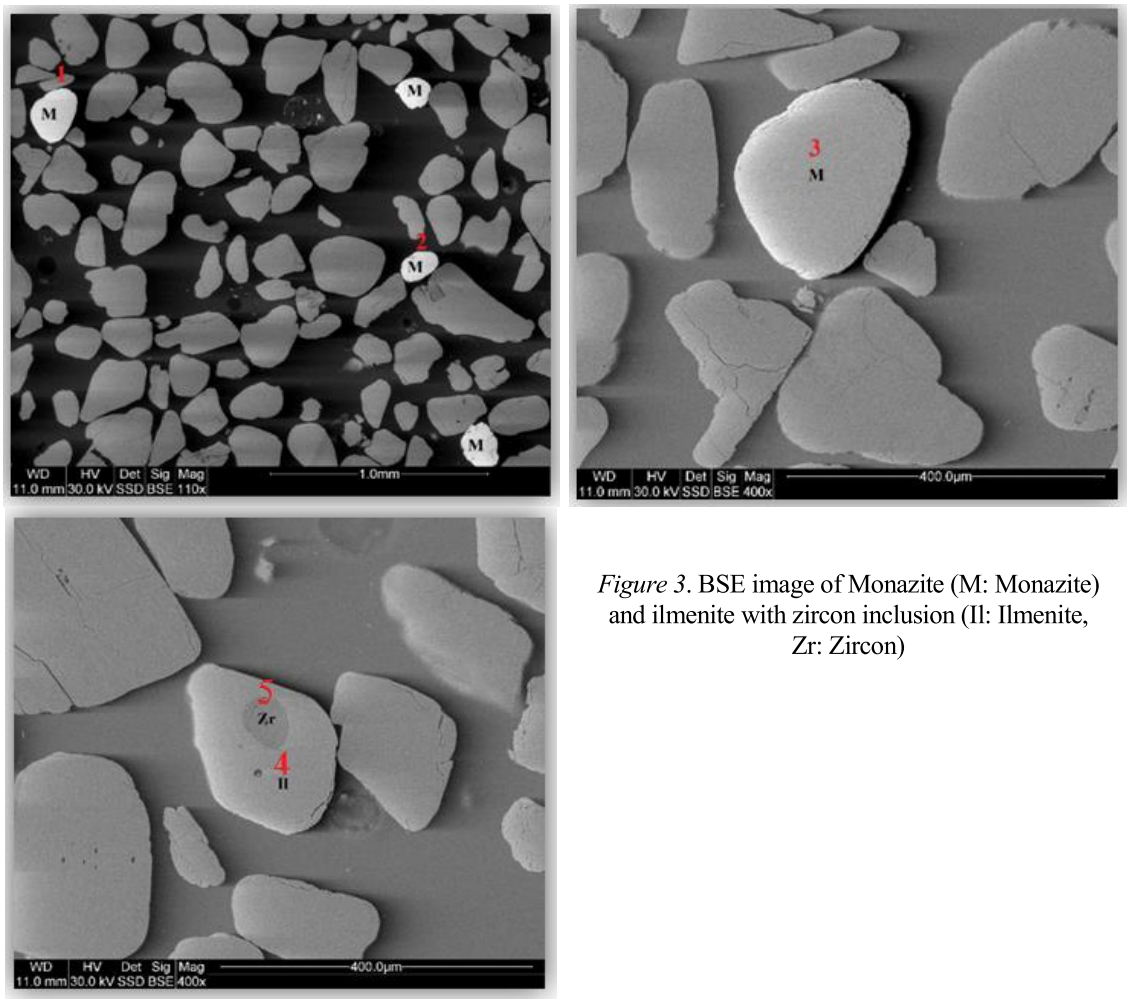

Figure 3. BSE image of Monazite (M: Monazite) and ilmenite with zircon inclusion (Il: Ilmenite, Zr: Zircon)

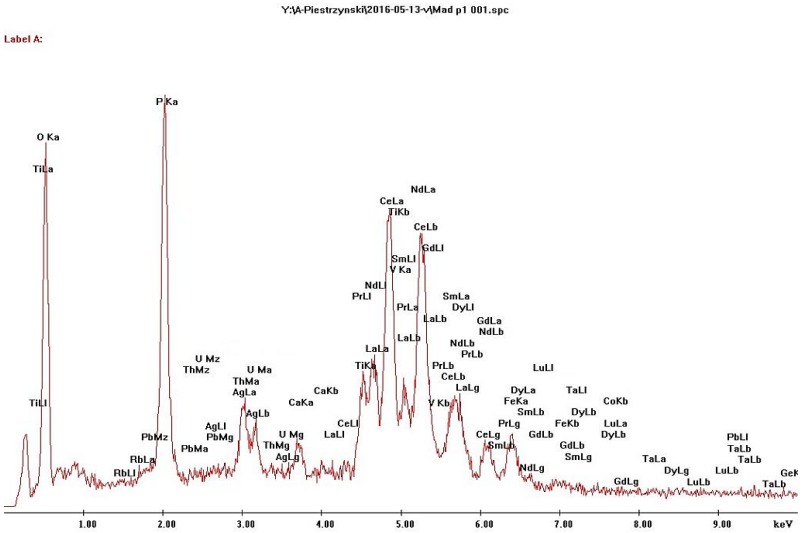

Figure 4. Graph of EDS results Monazite (number point 1)

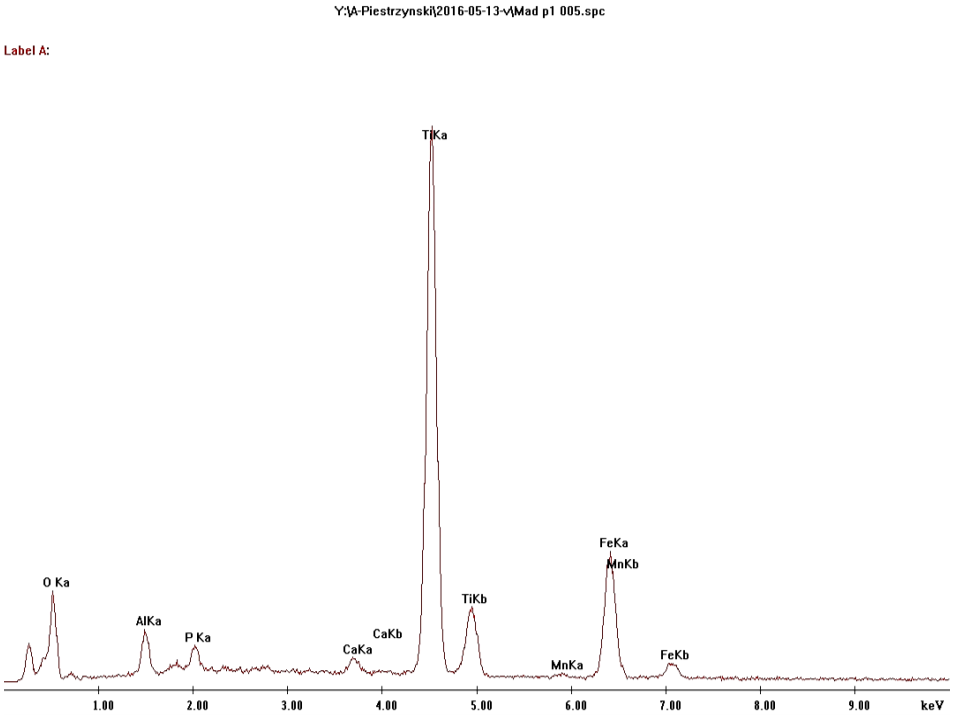

Figure 5a. Graph of EDS result Ilmenite

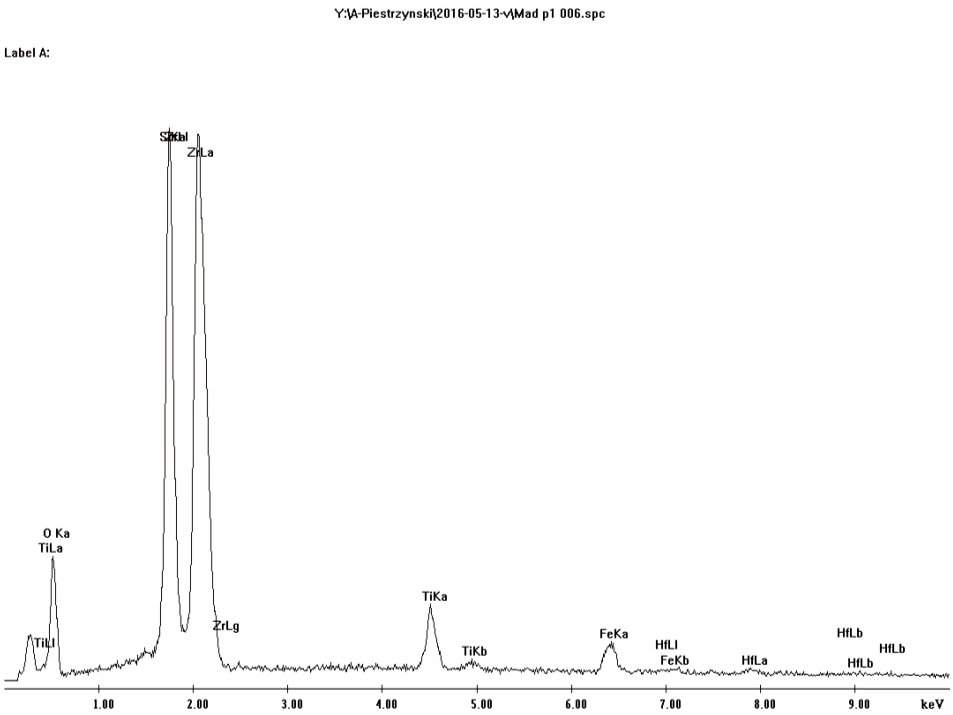

Figure 5b. Graph of EDS result Zircon

The concentration of 238U and 232Th measured by gamma-ray spectrometer are approximately 0.012–0.034 wt.% in 238U and ~0.27–0.60 wt.% in 232Th. But counting the amount of U and Th isotopes contribution in monazite approximated to 0.033 and 0.2 wt.% respectively. So the concentration of all Th isotopes in monazite just occupies about 50 % isotopes of 232Th measured by the gamma-ray spectrometer in sand samples while almost U content is contributed in monazite.

4.3. Chemical characteristic

The max, min and average concentrations of the major, trace and REE in the selected samples collected from the studied area are summarized in Table 1. The results show the major elements are Ti, Fe, Si, Al, Mg, Ca, P, Na, K., In general, the sand placer is very rich in Ti and Fe contents which reach 25.5% and 20.6% respectively. The remain of major elements is less than 1%. The trace elements vary in range from few to thousand ppm, in their Mn, Nb, and Zr is dominant with the Zr concentration reaches up to very high of 31000 ppm and 10630 ppm on average.

The deposited material is very rich in Σ REE up to 16000 ppm with very high Σ LREE/Σ HREE ratio is more than 31 (the result can say the principal REE is especially LREE), it could suggest the origin of material of sand placer from the weathering processes on the igneous magmatic formations. The Ce and La elements are the highest rare earth elements in comparison with other REE.

5. Conclusions

The Fort-Dauphin beach sand placer is significantly enriched in heavy minerals include zircon, garnet, spinel, sillimanite, monazite, anatase, rutile, titanite, leucoxene, pseudorutile and ilmenite. The economic heavy minerals in the sands are ilmenite, monazite, and zircon.

Chemical characteristic of the beach sand placer: Ti and Fe are the main major elements; the sand does not only reach in REE (total REE up to 16000 ppm) but also rich in Zr element (up to 31000 ppm), and the LREE is principal REEs with the high ratio of Σ LREE/Σ HREE >31.

Natural radionuclides are the richest especially in monazite and they could reach 10 wt.% in total. It could be one of the principal reasons, to contribute a very high natural radioactive background in the studied area. The main natural radionuclide is 238Th which the concentration is up to 6000 ppm and 3610 ppm on average.

Acknowledgments

The authors thank Prof. Nguyen Dinh Chau, Prof. Jaroslav Prsek and Dr. Jodłowski Paweł for their discussion, comments and support in the laboratory of Faculty of Physics and Applied Computer Science and Faculty of Geology, Geophysics and Environmental Protection in AGH UST, Krakow, Poland. Trinh PT thanks the assistance of Senior Research Project, VAST, code NVCC 11.01/20-20.6.

References

Abd E.W.M, El N.H.A., 2013. Radionuclides measurements and mineralogical studies on beach sands, East Rosetta Estuary, Egypt. Chin. J. Geochem., 32, 146–156.

Alam M.N., Chowdhury M.I., Kamal M., Ghose S., Islam M.N., Mustafa M.N., Miah M.M.H., Ansary M.M., 1999. The ^{226}Ra, ^{232}Th and ^{40}K activities in Beach Sand minerals and beach soils of Cox's Bazar, Bangladesh. J. Environ. Radioact., 46, 243–250.

Alencar A.S and Freitas A.C., 2005. Reference levels of natural radioactivity for the beach sands in a Brazilian southeastern coastal region. Radiation Measurements, 40, 76–83.

Almayahi B.A., Tajuddin A.A., Jaafar M.S., 2012. Effect of the natural radioactivity concentrations and ^{226}Ra/^{238}U disequilibrium on cancer diseases in Penang, Malaysia. Radiation Physics and Chemistry., 81, 1547–1558.

Andriamanantena T., 2008. Evolution de la minéralisation en monazite le long de la vallée de l'Ifaho du massif de Manangotry (Chaines Anosyennes) jusqu'à la cote dans les environs de Taolagnaro, Ecole Supérieure Polytechnique d'Antananarivo, Dép. Géol. Mémoire de fin d'étude (in French).

Bazot G., 1974. Géologie de la Région de Fort Dauphin-Sainte Luce, Sud-Est de Madagascar, Service géologique Antananarivo. TBG, 142, 1–44 (in French).

De V.R.H., 1978. Uranium Geology and Exploration: Lecture Notes and References. Colorado School of Mines, Golden Colorado, 396p.

Dean M.H., Subhash J., Yanis M., 2011. The major rare-earth-element deposits of Australia: geological setting, exploration, and resources, 207p.

Elsner H., 2010. Heavy minerals of economic importance. Assessment manual. Bundesanstalt für Geowissenschaften und Rohstoffe (BGR) (Federal Institute for Geosciences and Natural Resources), 218p.

Freitas A.C., Alencar A.S., 2004. Gamma dose rates and distribution of natural radionuclides in sand beaches, Ilha Grande Southeastern Brazil. J. Environ. Radioact., 75, 211–223.

ICRP, 1983. Radionuclide transformations. Publication of International Commission on Radiological Protection. ICRP-38, 11–13.

International Atomic Energy Agency, 1989. Measurement of radionuclides in food and the environment. Technical report series, IAEA, Vienna, 295.

Jodlowski P., 2006. Self-absorption correction in gamma-ray spectrometry of environmental samples - an overview of methods and correction values obtained for the selected geometries. Nukleonika, 51(2), 21–25.

Jodlowski P., Kalita S., 2010. Gamma-Ray Spectrometry Laboratory for high-precision measurements of radionuclide concentrations in environmental samples. Nukleonika, 55(2), 143−148.

Lacroix A., 1922. Minéralogie de Madagascar, Tomes 1, Paris, Challamel A. Ed. (in French).

Lange R., 1972. Geochemical Tables, Edition Leipzig.

Mohanty A.K., Das S.K., Van K.V., Sengupta D., Saha S. K., 2003a. Radiogenic heavy minerals in Chhatrapur beach placer deposit of Orissa, southeastern coast of India. Journal of Radioanalytical and Nuclear Chemistry, 258(2), 383–389.

Mohanty A.K., Das S.K., Van K.V., Sengupta D., Saha S.K., 2003b. Geochemical studies of monazite sands of Chhatrapur beach placer deposit of Orissa, India by PIXE and EDXRF method. Nuclear Instruments and Methods in Physics Research, B(211), 145–154.

Mohanty A.K., Sengupta D., Das S.K., Saha S.K., Van K.V., 2004. Natural radioactivity and radiation exposure in the high background area at Chhatrapur beach placer deposit of Orissa, India. J. Environ. Radioact., 75, 15–33.

Nada, A., Abd E.M.T.M.,, Abu Z.H., El-Asy I.E., Mostafa S.M.I., Abd E.A S.A., 2012. Correlation between radionuclides associated with zircon and monazite in beach sand of Rosetta, Egypt. J. Radioanal Nucl Chem., 291, 601–610.

NCRP, 1987. Exposure of the population of the United States and Canada from natural background radiation. Report No. 94. National Council on Radiation Protection and Measurements, Bethesda, Maryland.

Nguyen D.C., Jodlowski P., Kalita S.J, Olko P., Chrusciel F., Maksymowicz A., Waligorski M., Bilski P., Budzanowski M., 2008a. Natural radiation and its hazard in copper ore mines in Poland. Acta Geophysica, 56, 505–517.

Nguyen D.C., Michalec B., 2009. Natural radioactivity in bottled natural spring mineral, and therapeutic waters in Poland. J of Radioanalytical & Nuclear Chemistry, 279, 121–129.

Nguyen D.C., Phon L.K., Jodlowski P., Jadwiga P., Adam P., Hao D.V., Jakub N., 2016. Natural Radioactivity at the Sin Quyen iron oxide copper gold deposit in North Vietnam. Acta Geophysica (in press).

Papadopoulos A., Christofides G., Koroneos A., Stoulos S., 2014a. Natural radioactivity distribution and gamma radiation exposure of beach sands from Sithonia Peninsula. Central Eur. J. Geosci., 6(2), 229–242.

Papadopoulos A., Koroneos A., Christofides G., Papadopoulou L., Tzifas I., Stoulos S., 2016. Assessment of gamma radiation exposure of beach sands in highly touristic areas associated with plutonic rocks of the Atticocycladic zone (Greece). Journal of Environmental Radioactivity, 162, 235–243.

Papadopoulos A., Koroneos A., Christofides G., Stoulos S., 2014b. Natural radioactivity distribution and gamma radiation exposure of beach sands close the granitoids of NE Chalkidiki, Greece. In: Proceedings of the 10th International Congress of the Hellenic Geographical Society, 805–814.

Papadopoulos A., Koroneos A., Christofides G., Stoulos S., 2015a. Natural radioactivity distribution and gamma radiation exposure at beach sands close to Kavala pluton, Greece. Open J. Geosci., 1, 407–422.

Papadopoulos A., Koroneos A., Christofides G., Stoulos S., 2015b. Natural radioactivity distribution and gamma radiation exposure of beach sands close to Maronia and Samothraki plutons, NE. Greece. Geol. Balc., 43(1e3), 99–107.

Pownceby and Johnson, 2014. Geometallurgy of Australian uranium deposits. Ore Geology Reviews, 56, 25–44.

Qu L., Yao D., Cong P., Xia N., 2008. Radioactivity concentrations in soils in the Qingdao area, China [J]. Annals of the New York Academy of Sciences: Environmental Challenges in the Pacific Basin., 1140, 308−314.

Sengupta D., Mohantya A.K., Das S.K., Saha S.K., 2005. Natural radioactivity in the high background radiation area at Erasama beach placer deposit of Orissa, India. International Congress Series., 1276, 210–211.

Strezov A., Nonova T., 2009. Influence of macroalgal diversity on accumulation of radionuclides and heavy metals in Bulgarian Black Sea ecosystems. Journal of Environ. Radioact., 100, 144−150.

Sulekha R.D., Sengupta R., Guin S.K., 2009. Natural radioactivity measurements in beach sand along southern coast of Orissa, eastern India. Environ Earth Sci., 59, 593–601.

Takayuki S., Mohammad R., Masafumi A., Taishi K., Ikuji T., Toshiyuki F., Mashrur Z.M., 2015. Laboratory Enrichment of Radioactive Assemblages and Estimation of Thorium and Uranium Radioactivity in Fractions Separated from Placer Sands in Southeast Bangladesh. Natural Resources Research., 24(2), 209–220.